Early decrease of type 1 cannabinoid receptor binding and phosphodiesterase 10A activity in vivo in R6/2 huntington mice

By Ooms M, Rietjens R, Rangarajan JR, Vunckx K, Valdeolivas S, Maes F, Himmelreich U, Fernandez-Ruiz J, Bormans G, Van Laere K, Casteels C

Published in Neurobiol Aging. 2014 Dec;35(12):2858-69.
doi: 10.1016/j.neurobiolaging.2014.06.010.

Early decrease of type 1 cannabinoid receptor binding and phosphodiesterase 10A activity in vivo in R6/2 huntington mice

Maarten Ooms[a,b], Roma Rietjens[b,c], Janaki Raman Rangarajan[d], Kathleen Vunckx[c], Sara Valdeolivas[e-g], Frederik Maes[d], Uwe Himmelreich[h], Javier Fernandez-Ruiz[e-g], Guy Bormans[a,b], Koen Van Laere[b,c] and Cindy Casteels[b,c]

[a] Laboratory for Radiopharmacy, KU Leuven, Belgium

[b] MoSAIC, Molecular Small Animal Imaging Centre, KU Leuven, Belgium

[c] Division of Nuclear Medicine, KU Leuven and University Hospital Leuven, Belgium

[d] KU Leuven Medical Image Computing (ESAT/PSI), Department of Electrical Engineering & Medical Imaging Research Center, University Hospital Leuven, Belgium

[e] Departamento de Bioquímica y Biología Molecular, Facultad de Medicina, Universidad Complutense, Madrid, Spain

[f] Centro de Investigación Biomédica en Red sobre Enfermedades Neurodegenerativas (CIBERNED), Spain

[g] Instituto Ramón y Cajal de Investigación Sanitaria (IRYCIS), Madrid, Spain

[h] Biomedical NMR Unit, KU Leuven, Belgium

Running title**:** *In vivo* CB1 and PDE10A mapping in R6/2 mice

Author for correspondence:

Cindy Casteels PhD, Division of Nuclear Medicine, University Hospital Gasthuisberg, Herestraat 49 bus 7003, 3000 Leuven, Belgium. Tel. +32-16-343715, Fax +32-16-343759. E-mail: cindy.casteels@med.kuleuven.be

Abstract

Purpose: Several lines of evidence imply early alterations in endocannabinoid and phosphodiesterase 10A (PDE10A) signaling in Huntington disease (HD). Using [^{18}F]MK-9470 and [^{18}F]JNJ42259152 small-animal PET, we investigated for the first time cerebral changes in type 1 cannabinoid (CB1) receptor binding and PDE10A levels *in vivo* in pre-, early- and late symptomatic HD (R6/2) mice, in relation to glucose metabolism ([^{18}F]FDG PET), brain morphology (MRI) and motor function. **Methods:** Ten R6/2 and 16 wild-type (WT) mice were investigated at 3 different time points between the age of 4 and 13 weeks. Parametric CB1 receptor and PDE10A images were anatomically standardized to Paxinos space and analyzed voxel-wise. Volumetric microMRI imaging was performed to assess HD pathology. **Results:** In R6/2 mice, CB1 receptor binding was decreased in comparison to WT in a cluster comprising the bilateral caudate-putamen, globus pallidus and thalamic nucleus at week 5 (-8.1±2.6%; $p=1.7.10^{-5}$). Longitudinal follow-up showed further progressive decline compared to controls in a cluster comprising the bilateral hippocampus, caudate-putamen, globus pallidus, superior colliculus, thalamic nucleus and cerebellum (late vs. presymptomatic age: -13.7±3.1% for R6/2 and +1.5±4.0% for WT; $p=1.9.10^{-5}$). In R6/2 mice, PDE10A binding potential also decreased over time, to reach significance at early and late symptomatic HD (late vs. presymptomatic age: -79.1±1.9% for R6/2 and +2.1±2.7% for WT; $p=1.5.10^{-4}$). The observed changes in CB1 receptor and PDE10A binding were correlated to anomalies exhibited by R6/2 animals in motor function, while no correlation was found with MRI-based striatal volume. **Conclusion:** Our findings point to early regional dysfunctions in endocannabinoid and PDE10A signaling, involving the caudate-putamen and lateral globus pallidus, that may play a role in the progression of the disease in R6/2 animals. PET quantification of *in vivo* CB1 and/or PDE10A binding may thus be useful early biomarkers for HD. Our results also provide evidence of subtle motor deficits at earlier stages than previously described.

Key Words: Type 1 cannabinoid receptor, phosphodiesterase 10A, Huntington disease, small-animal PET, R6/2 mice

1. Introduction

Huntington disease (HD) is an autosomal dominant inherited neurodegenerative disease, characterized by motor dysfunctions, behavioural changes and cognitive decline. The causative mutation is an expanded CAG repeat in exon 1 of the gene encoding the protein huntingtin (htt) (The Huntington's Disease Collaborative Research Group, 1993). Adult onset is usually observed with trinucleotide repeat blocks between 40 and 50 units, whereas more than 60 repeat results in more severe and much less frequently observed juvenile, and even infantile, forms. The most striking pathophysiological feature of HD affected brains is the progressive atrophy of the caudate nucleus and the putamen, accompanied by a secondary enlargement of the lateral ventricles, and cortical degeneration in some patients (Vonsattel et al., 1985). Despite progress in elucidating the molecular pathology of HD, therapeutic benefit for patients in terms of effective pharmacotherapy with either symptomatic or protective effects, has been scarce.

The type 1 cannabinoid (CB1) receptor and phosphodiesterase 10A (PDE10A) enzyme play a role in changed neurotransmission in HD (Hebb et al., 2004;Katona and Freund, 2008). CB1 receptors presynaptically modulate the release of other neurotransmitters (Goutopoulos and Makriyannis, 2002) and are found at high densities on GABA-ergic striatal projection neurons (Richfield and Herkenham, 1994). PDE10A hydrolyzes the important second messengers cyclic adenosine monophosphate (cAMP) and cyclic guanosine monophosphate (cGMP), and is characterized by a restricted distribution, predominantly in medium spiny neurons of the striatum (Seeger et al., 2003). In HD, loss of CB1 receptor binding and/or signalling from the basal ganglia nuclei is one of the earliest neurochemical alterations observed in humans (Richfield and Herkenham, 1994;Glass et al., 2000;Allen et al., 2009) and experimental models (Denovan-Wright and Robertson, 2000;Lastres-Becker et al., 2002;Lastres-Becker et al., 2004;Centonze et al., 2005;Dowie et al., 2009;Blazquez et al., 2011), preceding the development of cerebral metabolic deficits (Antonini et al., 1996) and striatal volume losses (Glass et al., 2000). Also, decreased levels of PDE10A expression occur prior to the onset of motor-related HD symptoms in transgenic HD mice (Hebb et al., 2004). In addition, genetic ablation of CB1 receptors showed to accelerate the onset of HD-like symptoms in transgenic R6/2 mice (Blazquez et al., 2011), while PDE10A inhibition ameliorated striatal and cortical pathology in experimental HD (Giampa et al., 2010;Kleiman et al., 2011;Giralt et al., 2013). Furthermore,

pharmacological studies demonstrated crosstalk of CB1 and PDE10A with striatal dopaminergic signalling (Nishi et al., 2008;Chiang et al., 2013). In symptomatic HD patients, we found a profound cortical and subcortical loss of CB1 receptor availability *in vivo* (Van Laere et al., 2010).

So far, only *in vitro* and *ex vivo* data exist on the CB1 receptor binding and PDE10A activity in genetic HD models. *Ex vivo* studies of CB1 receptor changes in transgenic mouse models of HD have focused on the basal ganglia, hippocampus and motor cortex, but have not assessed other brain regions (Dowie et al., 2009;Dowie et al., 2010). Also it remains unknown whether CB1 receptor and PDE10A levels are changed *in vivo*, and to what spatial and temporal extent. Thanks to the development of selective CB1 ([^{18}F]MK-9470, (Burns et al., 2007)) and PDE10A radioligands ([^{18}F]JNJ42259152, (Celen et al., 2013)), *in vivo* imaging of these proteins became feasible.

Our primary objective was thus to investigate CB1 receptor and PDE10A changes *in vivo* throughout the disease process of R6/2 transgenic HD mice. As second objective, motor function, brain glucose metabolism and morphology, all shown to be altered (early) in patients and animal models of HD (Antonini et al., 1996;Carter et al., 1999;Cowin et al., 2011;Rattray et al., 2013), were investigated in the same animals and correlated to the regional CB1 receptor binding and PDE10A levels.

2. Materials and methods

2.1 Animals

Heterozygous male and female mice transgenic for exon 1 of the human HD gene with a greatly expanded CAG repeat (R6/2 mice; C57BL/6 background) (Mangiarini et al., 1996) and wild-type (WT) littermates were obtained from a Jackson Laboratories (Bar Harbour, Maine, USA) colony, developed at the Complutense University of Madrid, Spain. In total, 7 transgenic HD (R6/2) female, 3 R6/2 male, 10 female and 6 male WT mice were bred. All mice were housed per 3 or 4, with the same gender and genotype. Housing conditions were standard (12-hr light/dark cycle) and animals had *ad libitum* access to food and water. Mice were allowed several days of habituation and were used between 4-13 weeks of age, a range that corresponds to the pre-symptomatic phase extending to the advanced

stage of HD (Carter et al., 1999). Animal use and care followed the European Communities Council Directives (86/609/EEC).

2.2 Radiotracer preparation

Brain CB1 receptor imaging was done using the radioligand [^{18}F]MK-9470 (N-[2-(3-cyanophenyl)-3-(4-(2-[^{18}F]fluorethoxy)-phenyl)-1-methylpropyl]-2-(5-methyl-2-pyridyloxy)-2-methylpropona-mide), which is characterized by high specificity and high affinity for the CB1 receptor (rat Ki 0.7nM) (Casteels et al., 2012). The precursor for [^{18}F]MK-9470 was obtained from Merck Research Laboratories (MRL, West Point, USA). Radiolabeling was performed onsite by alkylation of the precursor with 2-[^{18}F]fluoroethylbromide, as previously described in (Burns et al., 2007). Brain PDE10A imaging was done using the radioligand [^{18}F]JNJ42259152 (rat IC_{50} 1.6 nM) (Celen et al., 2010). Its precursor was obtained from Janssen Research and Development (Beerse, Belgium). Radiolabeling was done by alkylation of the precursor with [^{18}F]fluoroethylbromide (Andres et al., 2011). In addition, glucose metabolism was quantified using [^{18}F]FDG. [^{18}F]FDG was prepared using a Cyclone 18/9 cyclotron and a routine [^{18}F]FDG synthesis module (IBA, Louvain-la-Neuve, Belgium). All tracers were produced with a radiochemical purity of > 95% and a specific activity range of 95 – 534 GBq/µmol at end of synthesis.

2.3 Small-animal PET imaging

Functional imaging of brain CB1 receptor binding, PDE10A enzyme activity and glucose metabolism was performed in R6/2 and WT animals at the age of 4-5, 7-8 and 11-12 weeks to study the pre-, early and late symptomatic phase, respectively (for time-line overview, see Fig. 1). Prior to small-animal PET imaging, mice were anesthetized using 2% isoflurane in 2.0 L/min oxygen. Tail veins were catheterized for injection of the radioligands ([^{18}F]MK-9470 9.3±1.6 MBq; [^{18}F]JNJ42259152 7.4±2.3 MBq and [^{18}F]FDG 11.7±1.4 MBq; mass dose per body weight: 0.5±0.2 nmol/kg). The radioligands were injected in a total volume of approximately 300 µL. [^{18}F]MK-9470 activity measurements were obtained after overnight fasting during a 20-min interval, starting 1 h post-injection, as previously validated in (Casteels et al., 2012), while [^{18}F]FDG acquisitions were performed dynamically for 90 min (Casteels et al., 2013). [^{18}F]JNJ42259152 acquisitions were done dynamically for 60 min without overnight fasting (Celen et al., 2013). All small-animal PET data for one time point were acquired

within a time span of 1 week. Small-animal PET imaging was performed using a FOCUS 220 tomograph (Siemens/Concorde Microsystems, Knoxville, TN), which has a transaxial resolution of 1.35 mm full-width at half-maximum. Data were reconstructed in a 256×256×95 matrix with a pixel width of 0.316 mm and a slice thickness of 0.796 mm.

To assess atrophy of the caudate-putamen (Sawiak et al., 2009;Rattray et al., 2013), anatomical MRI was performed in the same week as PET on a 9.4 Tesla Bruker Biospec Scanner (Bruker Biospin, Ettlingen, Germany) using a dedicated mouse brain surface coil (Rapid Biomedical, Rimpar, Germany). Three-dimensional high resolution images of the entire mouse brain were obtained in 20 min using a conventional 3D turboRARE sequence with following parameters: TR=1300 ms, TE=14.2 ms, rare-factor=16, matrix 192x256x128, isotropic voxel size of 80 µm. Mice were anesthetized with 1.5–2% isoflurane, the head fixed in a stereotaxic frame and body temperature maintained at 37±1 °C.

2.4 Image processing and data analysis

For quantification purposes, PET scans were reconstructed using an iterative maximum a posteriori probability algorithm with ordered subsets (MAP; 18 iterations, 9 subsets, fixed resolution: 1.5 mm) (Qi et al., 1998). SUV images of [^{18}F]MK-9470 binding based on standard uptake values (SUV=activity concentration (MBq/ml) x body mass (g) / injected dose (MBq)) were generated as measure of absolute [^{18}F]MK-9470 binding. SUV was previously validated to give good estimates of total receptor volume of distribution as determined by full kinetic modeling in rats (Casteels et al., 2012). We investigated relative [^{18}F]MK-9470 binding as well to exclude the higher physiologic interindividual variability of absolute [^{18}F]MK-9470 determinations in the brain. Relative [^{18}F]MK-9470 binding have the advantage of being much more sensitive, allowing changes of 5–10% to be measured using SPM (Van Laere et al., 2002). Relative [^{18}F]MK-9470 binding was expressed as SUV normalized on whole-brain SUV. For PDE10A, voxelwise parametric binding potential (BP_{ND}) images were reconstructed using a Logan reference tissue model using the cerebellum as reference region in PMODv.3.1 (PMOD Inc, Zurich, Switzerland), as previously validated in (Celen et al., 2013). Glucose metabolism was determined by normalizing [^{18}F]FDG data from the 45-60 min time interval to the whole-brain uptake in that time frame (Poisnel et al., 2012).

To obtain maximal use of information without a priori knowledge, PET data were analyzed voxel-wise using SPM8 (Statistical Parametric Mapping, Wellcome Department of Cognitive Neurology, London,

UK). For spatial normalization, individual PET data were manually normalized using affine transformations to tracer-specific custom-made mouse brain PET templates in Paxinos stereotactic space (Casteels et al., 2013). This methodology allows reporting results in coordinates directly corresponding to the Paxinos coordinate system for the mouse brain.

For SPM analysis, data were analyzed in a flexible factorial design using subjects (R6/2 vs. WT) x conditions (4-5 weeks vs. 7-8 weeks vs. 11-12 weeks). T-maps were interrogated at a peak voxel threshold (height/amplitude) of p_{height}=0.005 (uncorrected) and extent threshold k_E>200 voxels. Only significant clusters with $p_{cluster}$<0.05 (corrected for multiple comparisons) were retained, in combination with sufficient localizing power (p_{height}<0.005, uncorrected for multiple comparisons) (Casteels et al., 2011;Luyten et al., 2012). These p-values were set prior to SPM analysis using a Monte Carlo simulation (AlphaSim, AFNI, http://afni.nimh.nih.gov/afni) to ensure that family-wise error was kept below 5%. For analysis of relative CB1 receptor binding and relative glucose metabolism, proportional scaling to the mean voxel value was used and an analysis threshold of 0.8 of the mean image intensity was applied. To exclude the influence of gender, analyses were done with this variable as covariate. In addition, a voxel-based correlation analysis between relative CB1 receptor binding/ PDE10A BP_{ND}/ [^{18}F]FDG uptake and the behavioral outcomes for motor function was performed.

To assess the volumetric loss of HD *in vivo*, caudate-putamen volume was delineated automatically from the 3D turboRARE MR images (Sawiak et al., 2009;Rattray et al., 2013). For this purpose, all MR images were corrected for RF inhomogeneity (Likar et al., 2001) and spatially aligned by affine registration to a custom-made MRI template in Paxinos space (Casteels et al., 2013) using maximization of mutual information (MMI) criteria (Maes et al., 1997). In order to model the regional atrophy in HD animals, affine transformations were supplemented by B-spline based deformable registration (Loeckx et al., 2003) using a spline degree of 2, and isotropic mesh size of 0.64 mm. Based on the transformation determined by this spatial normalization step, predefined delineations of caudate-putamen on the MR template were propagated to individual MR images and used as measure of caudate-putamen volume. Any CSF contrast falsely included in the segmented caudate-putamen volume was systematically removed in all images using low-level intensity thresholding.

Individual labels of caudate-putamen volume were also propagated to individual PET data upon rigid manual PET-MRI registrations. The PET quantification using these individual labels of caudate-

putamen volume was subsequently compared to the PET quantification by aid of a pre-defined VOI map in Paxinos space (Casteels et al., 2013), to assess impact of morphological changes on caudate-putamen quantitative outcomes.

2.5 Motor testing

All mice were tested within the light phase of a 12h light/dark cycle for motor function using the rotarod, Catwalk™ and horizontal ladder test, as described below. Motor function was tested at the age of 6, 9 and 13 weeks, i.e. within 1-2 weeks from the small-animal PET experiments (for time-line overview, see Fig.1).

2.5.1 Rotarod

To assess motor coordination and balance in R6/2 and WT animals, mice were trained to remain on a fixed speed rotarod, as previously reported in (Carter et al., 1999). All mice underwent a 3-day training program on a 3 cm diameter rotarod (Ugo Basil, Biological Research Apparatus, Varese, Italy). During the training period, each mouse was placed on the rotating cylinder at a constant speed (24 rotations per minute; rpm) for a maximum of 60 sec, and the latency to fall of the rotarod within this time period was recorded. Mice received 4 trials per day, for three consecutive days, by which time a steady baseline level of performance was attained. The test took place on the 4^{th} day and consisted of two trials at 5 different velocities, ranging from 16 rpm to 32 rpm. The latency to fall of the rotarod at each speed level was recorded. Data from the two trials on the test day were averaged per speed level and used in statistical analysis.

2.5.2 Catwalk™ quantitative gait analysis test

The Catwalk (Noldus, Wageningen, The Netherlands) consists of a horizontal glass plate and video-capturing equipment placed below. It allows semi-automated quantification of a large number of locomotor parameters during walkway crossing. Based on the position, pressure, and surface area of each footfall multiple parameters are calculated such as stride length, base of support, interlimb coordination, and swing/stance phases (Vandeputte et al., 2010). For correct locomotor analysis, three uninterrupted runs were used with a minimum of 3 step sequence patterns. Body mass as confounding variable was measured at all test days.

2.5.3 Horizontal ladder test

To assess skilled walking, limb placement and limb coordination, we performed the horizontal ladder test (HLT). The horizontal ladder rung walking test apparatus consisted of side walls made of clear Plexiglas and metal rungs (2 mm diameter) which could be inserted to create a floor with a minimum distance of 0.4 cm between rungs. The side walls were 50 cm long and 10 cm high measured from the height of the rungs. The entire apparatus was placed on two standard rat housing cages, 15 cm above the ground. The width of the alley was adjusted to the size of the animal, so that it was about 0.5 cm wider than an animal to prevent the animal from turning around. The difficulty of the task was modified by varying the position of the metal rungs. Animals were tested in two ladder conditions, a regular pattern and an irregular random pattern. In the regular pattern, rungs were arranged at a distance of 0.4 cm apart. In the irregular pattern, the distance of the rungs varied, ranging from 0.4 to 3.2 cm. A camera (GZ-MG335, HD Everio, JVC) was positioned at a slight ventral angle, so that both sides of the body and paw positions could be recorded simultaneously from a ventral view.

Prior to testing, animals were trained to cross the ladder from the beginning to the end of the ladder. All animals crossed the ladder in the same direction. No reinforcement was given to motivate the animals to cross the ladder. All animals were trained on the regular rung pattern for five times per session, for two consecutive days. The next day, animals were tested 3 times on the regular rung pattern, and 3 times on the irregular rung pattern. Only the test session was filmed. All video recordings were analyzed frame-by-frame. Each step during a pass along the ladder was scored, however, the first two initiation steps and last two final steps were omitted when an animal paused. Each correct and each incorrect step was scored using a 1 to 6 scoring scale as in (Metz and Whishaw, 2002b). The number of errors in each session and the error score that was calculated from the total number of errors and the number of steps for each limb were subsequently used as quantitative outcomes.

2.6 General statistics

Reported values in this manuscript are given as the mean±SD. Conventional statistics were carried out using Graphpad Prism 5.1 (Graphpad Software, La Jolla, CA, USA). Measurements of rotarod, horizontal ladder test and caudate-putamen volume were analyzed using 2-way ANOVA tests with Time and Genotype as between-subject factors. Bonferroni's post-hoc test was applied for multiple

comparisons. Catwalk data and body weight were analyzed using non-parametric Mann-Whitney U tests as time variations in size, weight and skeletal morphometry have been shown to influence standard gait parameters (Wooley et al., 2009). The spearman correlation analysis was used for all correlative tests. Significance was accepted at the 95% probability level.

3. Results

3.1 Small-animal [^{18}F]MK-9470, [^{18}F]JNJ42259152 and [^{18}F]FDG PET imaging

Absolute [^{18}F]MK-9470 binding values were not significantly different in the brain of R6/2 mice and WT littermates at the age of 5, 7 and 11 weeks. Also, absolute [^{18}F]MK-9470 values of C57BL/6 mice were consistent in magnitude with those previously reported in Wistar (Casteels et al., 2010a;Casteels et al., 2010b) and Sprague-Dawley rats (Casteels et al., 2011). Mean images of absolute [^{18}F]MK-9470 binding in the mouse brain of 11-week-old R6/2 mice and controls are shown in Figure 2A. As can be seen from this figure, the pattern of [^{18}F]MK-9470 binding observed in the mouse control brain is similar to that previously reported *ex vivo* (Herkenham et al., 1990), i.e. high uptake in the cortex, cerebellum, hippocampus and caudate-putamen.

In R6/2 mice, regional relative [^{18}F]MK-9470 binding was decreased in comparison to WT in the bilateral caudate-putamen, globus pallidus and thalamic nucleus at week 5 (-8.1±2.6%; -8.0±3.3% and -7.0%±2.2%, respectively, all $p \leq 2.0 \ .10^{-5}$). Longitudinal follow-up showed further progressive decline between genotypes. Voxel-based analysis showed decreased binding in R6/2 mice vs. WT between week 5 and 7 in a cluster comprising the bilateral hippocampus, caudate-putamen, globus pallidus, superior colliculus, thalamic nucleus and cerebellum (Fig. 3A). The mean decrease at the Paxinos coordinate peak maximum was -11.6±2.0 % vs. +4.4±4.4 % ($p=1.1 \ .10^{-6}$) for R6/2 mice and WT, respectively. This decrease remained present at late symptomatic ages, predominantly in the left hemisphere (-13.7±3.1 % for R6/2 vs. +1.5±4.0 % for WT between week 11 and week 5; $p=1.9 \ .10^{-5}$; Fig. 3B).

Representative images of mean PDE10A BP_{ND} values in the caudate-putamen of 12-week-old R6/2 mice and controls for [^{18}F]JNJ42259152 are shown in Figure 2B. Voxel-based analysis demonstrated

decreased BP_{ND} values in the bilateral caudate-putamen of R6/2 mice in comparison to controls over time that reached significance at 12 weeks of age (Fig. 4A). The decrease at the Paxinos coordinate peak maximum was -67.9±0.1 % for the left caudate-putamen ($p=1.5\ .10^{-4}$) and -79.1±1.9 % for the right caudate-putamen ($p=2.9\ .10^{-4}$) in R6/2, while BP_{ND} values of WT animals changed non-significantly with -10.0±3.7% and +2.1±2.7%, respectively, between week 5 and week 12. Predefined VOI analysis in Paxinos space confirmed SPM findings of week 12, but also showed significantly decreased PDE10A binding at week 8 ($F_{(genotype\ x\ time)2,8} = 15.8$; $p<0.05$ week 8 and $p<0.001$ week 12, Fig. 4B).

For [^{18}F]FDG, no significant changes were detected between R6/2 and WT animals over time ($p_{height} <0.005$; $k_E >200$; Fig. 2C).

Above small-animal PET findings were also observed without a genotype x time-effect in caudate-putamen volume, although caudate-putamen volume of R6/2 mice was lower at week 13 in comparison to WT animals, i.e 24.8±1.0 mm³ vs. 26.1±0.9 mm³ (2-way ANOVA, NS).

Detailed cluster peak locations and p-values of all SPM findings at the SPM analysis threshold, i.e. $p_{height} \leq 0.005$ uncorrected, $k_E > 200$, and $p_{cluster} < 0.05$ corrected, are shown in Table 1.

3.2 Motor testing

Throughout the study, control mice maintained longer times on the rotarod at all rotation speeds. In R6/2 mice, there was a progressive decline in performance over time at all 5 speeds (Fig.5). Significant deficits were present for each velocity at 13 weeks of age (2-way ANOVA, $p<0.05$). At the highest velocity (32 rpm) performance of R6/2 mice decreased by 62.0% compared to WT ($F_{(genotype\ x\ time)2,54} = 7.3$; $p<0.01$).

On the Catwalk, transgenic mice showed comparable results to controls at 6 weeks and 9 weeks of age. At 13 weeks of age, however, R6/2 mice showed a lower swing speed (range: -31.1%, -47.9%; $F(genotype)_{1,36} = 21.4$; $p<0.001$) and shorter stride lengths (range: -25.8%, -34.8%; $F(genotype)_{1,36} = 42.1$; $p<0.001$), while the duration of paw contact, i.e. stand (range: +47.5%, +89.3%;($F(genotype)_{1,36} = 24.8$; $p<0.001$) and print area (range: +37.2%, +204.1%;$F(genotype)_{1,36} = 11.9$; $p<0.01$) were

increased as compared to WTs for all paws (Fig. 6A-B). Absolute values of body mass did not significantly differ between genotypes at week 13 (p=0.1, NS)

In addition, the number of errors made using the front paws on an irregular ladder design was higher at each time point for R6/2 mice (e.g. +51.1% at week 6; $F_{(genotype)1,54}$ = 7.9; p<0.01), but it did not progress over time. A similar genotype-effect was observed when the error score was used as quantitative outcome (e.g. -12.3% at week 6; $F_{(genotype)1,54}$ = 8.8; p<0.01, Fig. 6C).

3.3 Correlation analysis of [^{18}F]MK-9470 and [^{18}F]JNJ42259152 with motor testing and striatal volume

Voxel-based correlation analysis showed a positive correlation between the latency to fall off the rotarod and relative [^{18}F]MK-9470 binding in a cluster covering the bilateral hippocampus and primary sensory cortex (spearman r=0.81, p<0.0004; Fig. 7A-B and Table 1). VOI-based PDE10A BP_{ND} values of the right caudate-putamen inversely correlated to the print area and duration of paw contact of the left forepaw while crossing the Catwalk (Fig. 7C-D; both spearman r = -0.86; p<0.02 corrected).

No correlations of relative [^{18}F]MK-9470 binding and PDE10A BP_{ND} values of the caudate-putamen with MRI-based striatal volume were observed, nor between relative [^{18}F]MK-9470 binding and PDE10A BP_{ND} values itself. Caudate-putamen values of absolute [^{18}F]MK-9470 binding and PDE10A BP_{ND} determined by the individual MR-based segmentation highly correlated to the ones obtained using a predefined VOI map oriented in Paxinos space, pointing to a limited influence of striatal volume changes on our quantitative outcomes (Fig. 7E-F; [^{18}F]MK-9470: spearman r=0.94, p<0.0001 and PDE10A: spearman r=0.97, p<0.0001).

4. Discussion

In this study, we have for the first time characterized CB1 receptor and PDE10A alterations *in vivo* in R6/2 transgenic mice of HD using [^{18}F]MK-9470 and [^{18}F]JNJ42259152 small-animal PET. We showed that in early and late stages of the symptomatic phase, both CB1 receptor binding and levels of PDE10A are decreased in basal ganglia regions.

Specifically for [^{18}F]MK-9470, at all studied ages, CB1 receptor binding was reduced in the caudate-putamen and globus pallidus of transgenic mice, where cell bodies and axon terminals of CB1 receptor-positive medium spiny neurons are located, respectively. Reduced binding of [^{18}F]MK-9470 to the CB1 receptor was also seen in the hippocampus, thalamic nucleus, superior colliculus and cerebellum at symptomatic ages. Reduction in CB1 receptor binding of basal ganglia regions is in line with *ex vivo* observations in R6/2 mice (Horne et al., 2013). Horne et al. found a 16% and 26% reduction in the striatal and pallidal CB1 receptor binding of 12-week-old R6/2 mice using immunohistochemistry. They did not – in contrast to this study - observe any change in protein binding at earlier time points. It has been reported that CB1 receptor downregulation in these regions primarily occurred in medium-sized spiny neurons belonging to the indirect pathway (Chiodi et al., 2012;Horne et al., 2013), a neuronal subpopulation also particularly vulnerable in HD patients (Reiner et al., 1988). CB1 receptor downregulation also occurred in neuropeptide Y / neuronal nitric oxide synthase-expressing interneurons of the striatum (Chiodi et al., 2012;Horne et al., 2013). In line with Horne et al., we also observed that the loss of striatal CB1 receptor binding is less pronounced compared with the loss of previously published CB1 receptor mRNA data in that region (Denovan-Wright and Robertson, 2000;Luthi-Carter et al., 2000;McCaw et al., 2004). These previous studies showed that striatal mRNA levels of the CB1 receptor decrease in R6/2 mice compared to wild-type animals from 3 weeks of age to a minimum level of ~30% by 4 weeks of age and remained constant thereafter (McCaw et al., 2004).

We also found reduced binding of [^{18}F]MK-9470 in other brain regions, especially the hippocampus, cerebellum and thalamic nucleus, a fact also found in HD patients given the ubiquitous expression of mutant htt that converts the disease multifactorial with symptoms (cognitive decline) and deterioration in cortical and subcortical (e.g. hippocampus) structures (Ross and Tabrizi, 2011). Similar observations have been done in transgenic mice, for example, symptomatic R6/2 mice are characterized by loss of CB1 receptor mRNA in a subset of hippocampal neurons (Denovan-Wright and Robertson, 2000) and by slightly reduced levels of the endogenous ligands, AEA and 2-AG (Bisogno et al., 2008). Also, disturbed functioning of Purkinje cells in which CB1 receptors are located at the synapses (Suarez et al., 2008), have been described in this model prior to cell loss (Dougherty et al., 2012). Cerebellar dysfunction is not surprising, knowing that R6/2 mice more closely replicate juvenile HD (Sawiak et al., 2009) and several reports have proved the occurrence of cerebellum-

related symptoms (e.g. ataxia) in these most severe HD patients (Ruocco et al., 2006;Nicolas et al., 2011). In addition, from an anatomical point of view, thalamic nuclei are connected to the striatum and participate in the control of voluntary movement. However, no preclinical data on CB1 receptor changes or endocannabinoid changes have been reported yet in this region, though we observed a profound subcortical decrease in CB1 receptor binding in symptomatic HD patients *in vivo* (Van Laere et al., 2010).

Similar to CB1, PDE10A density was also found to decline in R6/2 mice. In 8- and 12- week-old animals, PDE10A binding quantified with [^{18}F]JNJ42259152 PET was reduced bilaterally in the striatum. These *in vivo* findings are in line with few *ex vivo* results obtained in the same model (Hebb et al., 2004). For example, Hebb et al. observed declining PDE10A mRNA levels in R6/2 mice that initiates at the age of 4 weeks and that reaches a stable value at 9 weeks of age. The lower mRNA levels resulted in PDE10A protein levels of ~70% lower at 9 weeks compared to 3 week-old R6/2 mice.

The mechanism by which HD promotes an early loss of CB1 receptors is suggested to be caused by interactions between mutant htt and nuclear transcription factors, similar to other key elements whose transcriptional regulation is affected by mutant htt (e.g. BDNF). Blazquez and coworkers showed in striatal cells that mutant htt, due to loss-of-function, down-regulates CB1 receptors through the inhibition of gene promoter activity via repressor element 1 silencing transcription factor and sensitizes cells to excitotoxic damage (Blazquez et al., 2011). The decrease in PDE10A – on the other hand - could conceivably be an indirect and compensating mechanism secondary to the loss of cAMP. Gines et al. showed impairment of cAMP signaling and gene transcription of its target molecule, cAMP response element binding protein (CREB), through arresting CREB-binding protein due to a gain-of-function of mutant htt (Gines et al., 2003). Reduced cAMP signaling has been hypothesized to contribute to neuronal loss (Klevytska et al., 2010), while PDE10A inhibition increased CREB-mediated signaling (Giralt et al., 2013) and thus plays a neuroprotective role. This CREB theory could also explain why PDE10A inhibition is beneficial (Giampa et al., 2010;Kleiman et al., 2011) and improves spatial and recognition memory in the R6/1 mouse model for HD (Giralt et al., 2013) despite the fact that PDE10A expression decreases during disease progression. However, a change in the cellular localization of PDE10A (Leuti et al., 2013) or direct interference of mutant htt with PDE10A

transcription factors (Hu et al., 2004) cannot be excluded. The fact that alterations in CB1 receptor occurred slightly earlier than alterations of PDE10A levels fits with the different independent underlying mechanisms, i.e. a direct effect of mhtt vs. a compensatory (indirect) effect of cAMP, respectively.

In our work, we also demonstrated that changes in relative [^{18}F]MK-9470 binding of the bilateral hippocampus positively correlated to the rotarod performance, suggesting that animals with the lowest binding were related to a worse functional outcome. In agreement with this finding, especially abnormalities in T2 relaxivity of hippocampus and not in striatum volume have previously shown to be associated with rotarod performance in male and female R6/2 mice (Rattray et al., 2013). We also found that PDE10A BP_{ND} values of the right caudate-putamen correlated to the print area and duration of paw contact of the left forepaw. Although there is no evidence of asymmetry in the pathology of HD, our data do suggest that PDE10A of the right caudate-putamen is more associated with motor deficits, in particular with the control of the forepaw rather than of the hindpaw. Values of PDE10A BP_{ND} and [^{18}F]MK-9470 in the caudate-putamen itself did not correlate to each other, nor did we observe differences in [^{18}F]FDG uptake at symptomatic ages, similar to tgHD rats (Casteels et al., 2011). Nevertheless, our findings of an early *in vivo* loss of CB1 receptors and PDE10A enzyme, and their correlations with behavior – although modest - suggest that both [^{18}F]MK-9470 and [^{18}F]JNJ42259152 may be useful as early biomarkers of HD. Also, their decrease with age, though more narrow for CB1 receptors, suggests usefulness for testing potential therapeutic approaches aimed at delaying the onset and slowing down the disease progression. In line with this, inhibition of PDE10A showed to ameliorate striatal pathology and to delay disease onset in R6 mice (Giampa et al., 2010;Giralt et al., 2013). Also, CB1 receptor deletion showed to aggravate symptoms and the neuropathology of HD, while the pharmacological administration of the cannabinoid Δ9-tetrahydrocannabinol exerted a therapeutic effect and ameliorated above parameters (Blazquez et al., 2011). The more narrow age effect of CB1 receptors as compared to PDE10A could to some extent also be due to their abundant expression throughout the entire brain combined with the partial volume effect of small-animal PET imaging.

With respect to behavioral testing, it appeared that the horizontal ladder test is most sensitive in discriminating R6/2 mice from WT littermates, although their performance over time did not progress differently, indicating that dysfunctions/degeneration of the medium-sized spiny neurons minimally influenced our outcome. At each time point investigated, the numbers of errors made and the error

score using the front paws on an irregular ladder design was higher and lower, respectively, in R6/2 mice. This early discriminatory power is not surprising, knowing that the horizontal ladder test has proven sufficiently challenging to reveal subtle impairments in for- and hindlimb use and unmask impairments that require forebrain control (Metz and Whishaw, 2002a). Especially, using the irregular rung condition, mice are not capable of anticipating the rung location and learning a specific gait pattern. The horizontal ladder test has also proven sensitive to normal ageing as older rats showed more impaired rung walking than younger ones (Metz and Whishaw, 2002a), similar to what we observed in the present work. In addition, we succeeded in monitoring the progressive decline in motor performance that is characteristic of R6/2 mice using an incremental fixed speed rotarod protocol, as previously published (Carter et al., 1999;Samadi et al., 2013). Optimal rotation speeds for evaluating motor performance using this protocol were in the 20-32 rpm range, with the highest sensitivity at the highest speed. Using 32 rpm, impairments in performance became already apparent at 9 weeks, while only by the age of 13 weeks for all other speeds. However, we probably would have reached a higher sensitivity by the use of an accelerating rotarod. Previous data making use of continuously increasing speeds have reported on mild impairments in performances as early as 6-7 weeks of age (Luesse et al., 2001;Blazquez et al., 2011;Rattray et al., 2013;Petr et al., 2013). Using the Catwalk, deficiencies in gait were also detectable by 13 weeks of age; instead of walking in a straight line with evenly spaced and accurately positioned footprints, R6/2 mice showed reduced stride lengths and hypoactive behavior by decreased swing speed, increased print area and longer duration of paw contact. Notably, these abnormalities were similar to gait disturbances described in this model using the footprint test (Carter et al., 1999) and open field activity test (Samadi et al., 2013).

A major hallmark of HD is loss of projection neurons in the neostriatum, with relative sparing of interneuron subpopulations (Vonsattel et al., 1985). Initial studies in R6/2 mice demonstrated striatal atrophy (Reiner et al., 1988;Richfield et al., 1995), but later ones also reported on neuronal loss, which is first detectable at 11 weeks (Samadi et al., 2013). Since PDE10A is expressed in medium spiny neurons (Coskran et al., 2006), which are the most affected ones in HD, structural changes could potentially confound our findings. However, correcting for the striatal volume using MRI-based segmentation yielded similar results of decreased PDE10A binding over time in R6/2 animals and indicated a clear correlation between the data acquired by a predefined VOI map oriented in Paxinos space and individual MR-based segmentation in native space (r=0.97), pointing to limited influence.

Comparable findings were seen in the present work for absolute [^{18}F]MK-9470 binding in the caudate-putamen (r=0.94).

5. Conclusions

In vivo cerebral mapping of pre-, early- and late symptomatic mice transgenic for HD using [^{18}F]MK-9470 and [^{18}F]JNJ42259152 small-animal PET points to early regional dysfunctions in endocannabinoid and PDE10A signaling, incorporating the caudate-putamen. *In vivo* CB1 receptor and PDE10A enzyme measurements using [^{18}F]MK-9470 and [^{18}F]JNJ42259152 may thus be early biomarkers for HD. Translational studies in premanifest human carriers of the HD mutation using the same imaging techniques are needed to further demonstrate the clinical significance of this finding Our results also provide evidence of 1) *in vivo* CB1 receptor changes in the hippocampus, thalamic nucleus and cerebellum at symptomatic ages and of 2) subtle motor deficits at earlier stages than previously described.

6. Acknowledgements

We acknowledge Merck & Co, Inc. for the availability of the [^{18}F]MK-9470 precursor and Janssen Research and Development for the one of [^{18}F]JNJ42259152. The authors also thank Ann Van Santvoort and Julie Cornelis for their assistance in data acquisition, as well as the Leuven PET radiopharmacy team for tracer preparations. Financial support of the Fund for Scientific Research, Flanders, Belgium (FWO/G.0972.13), the KU Leuven *In Vivo* Molecular Imaging (IMIR) Consortium (KUL PF/10/017), and the European Commission (FP7, INMiND, grant agreement no. 278850) is gratefully acknowledged. Cindy Casteels and Kathleen Vunckx are supported by a post-doctoral mandate of the Research Foundation Flanders. Koen Van Laere is senior clinical investigator of the Research Foundation Flanders.

Conflict of interest

The authors declare that they have no conflict of interest.

7. References

Allen KL, Waldvogel HJ, Glass M, Faull RL (2009) Cannabinoid (CB(1)), GABA(A) and GABA(B) receptor subunit changes in the globus pallidus in Huntington's disease. J Chem Neuroanat 37:266-281.

Andres JI, De AM, Alcazar J, Iturrino L, Langlois X, Dedeurwaerdere S, Lenaerts I, Vanhoof G, Celen S, Bormans G (2011) Synthesis, in vivo occupancy, and radiolabeling of potent phosphodiesterase subtype-10 inhibitors as candidates for positron emission tomography imaging. J Med Chem 54:5820-5835.

Antonini A, Leenders KL, Spiegel R, Meier D, Vontobel P, Weigell-Weber M, Sanchez-Pernaute R, de Yebenez JG, Boesiger P, Weindl A, Maguire RP (1996) Striatal glucose metabolism and dopamine D2 receptor binding in asymptomatic gene carriers and patients with Huntington's disease. Brain 119 (Pt 6):2085-2095.

Bisogno T, Martire A, Petrosino S, Popoli P, Di Marzo V (2008) Symptom-related changes of endocannabinoid and palmitoylethanolamide levels in brain areas of R6/2 mice, a transgenic model of Huntington's disease. Neurochem Int 52:307-313.

Blazquez C, et al. (2011) Loss of striatal type 1 cannabinoid receptors is a key pathogenic factor in Huntington's disease. Brain 134:119-136.

Burns HD, et al. (2007) [18F]MK-9470, a positron emission tomography (PET) tracer for in vivo human PET brain imaging of the cannabinoid-1 receptor. Proc Natl Acad Sci U S A 104:9800-9805.

Carter RJ, Lione LA, Humby T, Mangiarini L, Mahal A, Bates GP, Dunnett SB, Morton AJ (1999) Characterization of progressive motor deficits in mice transgenic for the human Huntington's disease mutation. J Neurosci 19:3248-3257.

Casteels C, Koole M, Celen S, Bormans G, Van Laere K (2012) Preclinical evaluation and quantification of [(18)F]MK-9470 as a radioligand for PET imaging of the type 1 cannabinoid receptor in rat brain. Eur J Nucl Med Mol Imaging 39:1467-1477.

Casteels C, Lauwers E, Baitar A, Bormans G, Baekelandt V, Van Laere K (2010a) In vivo type 1 cannabinoid receptor mapping in the 6-hydroxydopamine lesion rat model of Parkinson's disease. Brain Res 1316:153-162.

Casteels C, Martinez E, Bormans G, Camon L, de Vera N, Baekelandt V, Planas AM, Van Laere K (2010b) Type 1 cannabinoid receptor mapping with [(18)F]MK-9470 PET in the rat brain after quinolinic acid lesion: a comparison to dopamine receptors and glucose metabolism. Eur J Nucl Med Mol Imaging 37:2354-2363.

Casteels C, Vandeputte C, Rangarajan JR, Dresselaers T, Riess O, Bormans G, Maes F, Himmelreich U, Nguyen H, Van Laere K (2011) Metabolic and type 1 cannabinoid receptor imaging of a transgenic rat model in the early phase of Huntington disease. Exp Neurol 229:440-449.

Casteels C, Vunckx K, Aelvoet SA, Baekelandt V, Bormans G, Van Laere K, Koole M (2013) Construction and evaluation of quantitative small-animal PET probabilistic atlases for [(1)(8)F]FDG and [(1)(8)F]FECT functional mapping of the mouse brain. PLoS One 8:e65286.

Celen S, Koole M, De Angelis M, Sannen I, Chitneni SK, Alcazar J, Dedeurwaerdere S, Moechars D, Schmidt M, Verbruggen A, Langlois X, Van Laere K, Andres JI, Bormans G (2010) Preclinical evaluation of 18F-JNJ41510417 as a radioligand for PET imaging of phosphodiesterase-10A in the brain. J Nucl Med 51:1584-1591.

Celen S, Koole M, Ooms M, De Angelis M, Sannen I, Cornelis J, Alcazar J, Schmidt M, Verbruggen A, Langlois X, Van Laere K, Andres JI, Bormans G (2013) Preclinical evaluation of [F]JNJ42259152 as a PET tracer for PDE10A. Neuroimage 82C:13-22.

Centonze D, Rossi S, Prosperetti C, Tscherter A, Bernardi G, Maccarrone M, Calabresi P (2005) Abnormal sensitivity to cannabinoid receptor stimulation might contribute to altered gamma-aminobutyric acid transmission in the striatum of R6/2 Huntington's disease mice. Biol Psychiatry 57:1583-1589.

Chiang YC, Lo YN, Chen JC (2013) Crosstalk between Dopamine D2 receptors and cannabinoid CB1 receptors regulates CNR1 promoter activity via ERK1/2 signaling. J Neurochem 127:163-176.

Chiodi V, Uchigashima M, Beggiato S, Ferrante A, Armida M, Martire A, Potenza RL, Ferraro L, Tanganelli S, Watanabe M, Domenici MR, Popoli P (2012) Unbalance of CB1 receptors expressed in GABAergic and glutamatergic neurons in a transgenic mouse model of Huntington's disease. Neurobiol Dis 45:983-991.

Coskran TM, Morton D, Menniti FS, Adamowicz WO, Kleiman RJ, Ryan AM, Strick CA, Schmidt CJ, Stephenson DT (2006) Immunohistochemical localization of phosphodiesterase 10A in multiple mammalian species. J Histochem Cytochem 54:1205-1213.

Cowin RM, Bui N, Graham D, Green JR, Grueninger S, Yuva-Paylor LA, Syed AU, Weiss A, Paylor R (2011) Onset and progression of behavioral and molecular phenotypes in a novel congenic R6/2 line exhibiting intergenerational CAG repeat stability. PLoS One 6:e28409.

Denovan-Wright EM, Robertson HA (2000) Cannabinoid receptor messenger RNA levels decrease in a subset of neurons of the lateral striatum, cortex and hippocampus of transgenic Huntington's disease mice. Neuroscience 98:705-713.

Dougherty SE, Reeves JL, Lucas EK, Gamble KL, Lesort M, Cowell RM (2012) Disruption of Purkinje cell function prior to huntingtin accumulation and cell loss in an animal model of Huntington disease. Exp Neurol 236:171-178.

Dowie MJ, Bradshaw HB, Howard ML, Nicholson LF, Faull RL, Hannan AJ, Glass M (2009) Altered CB1 receptor and endocannabinoid levels precede motor symptom onset in a transgenic mouse model of Huntington's disease. Neuroscience 163:456-465.

Dowie MJ, Howard ML, Nicholson LF, Faull RL, Hannan AJ, Glass M (2010) Behavioural and molecular consequences of chronic cannabinoid treatment in Huntington's disease transgenic mice. Neuroscience 170:324-336.

Giampa C, Laurenti D, Anzilotti S, Bernardi G, Menniti FS, Fusco FR (2010) Inhibition of the striatal specific phosphodiesterase PDE10A ameliorates striatal and cortical pathology in R6/2 mouse model of Huntington's disease. PLoS One 5:e13417.

Gines S, Ivanova E, Seong IS, Saura CA, MacDonald ME (2003) Enhanced Akt signaling is an early pro-survival response that reflects N-methyl-D-aspartate receptor activation in Huntington's disease knock-in striatal cells. J Biol Chem 278:50514-50522.

Giralt A, Saavedra A, Carreton O, Arumi H, Tyebji S, Alberch J, Perez-Navarro E (2013) PDE10 inhibition increases GluA1 and CREB phosphorylation and improves spatial and recognition memories in a Huntington's disease mouse model. Hippocampus 23:684-695.

Glass M, Dragunow M, Faull RL (2000) The pattern of neurodegeneration in Huntington's disease: a comparative study of cannabinoid, dopamine, adenosine and GABA(A) receptor alterations in the human basal ganglia in Huntington's disease. Neuroscience 97:505-519.

Goutopoulos A, Makriyannis A (2002) From cannabis to cannabinergics: new therapeutic opportunities. Pharmacol Ther 95:103-117.

Hebb AL, Robertson HA, ovan-Wright EM (2004) Striatal phosphodiesterase mRNA and protein levels are reduced in Huntington's disease transgenic mice prior to the onset of motor symptoms. Neuroscience 123:967-981.

Herkenham M, Lynn AB, Little MD, Johnson MR, Melvin LS, de Costa BR, Rice KC (1990) Cannabinoid receptor localization in brain. Proc Natl Acad Sci U S A 87:1932-1936.

Horne EA, Coy J, Swinney K, Fung S, Cherry AE, Marrs WR, Naydenov AV, Lin YH, Sun X, Keene CD, Grouzmann E, Muchowski P, Bates GP, Mackie K, Stella N (2013) Downregulation of cannabinoid receptor 1 from neuropeptide Y interneurons in the basal ganglia of patients with Huntington's disease and mouse models. Eur J Neurosci 37:429-440.

Hu H, McCaw EA, Hebb AL, Gomez GT, ovan-Wright EM (2004) Mutant huntingtin affects the rate of transcription of striatum-specific isoforms of phosphodiesterase 10A. Eur J Neurosci 20:3351-3363.

Katona I, Freund TF (2008) Endocannabinoid signaling as a synaptic circuit breaker in neurological disease. Nat Med 14:923-930.

Kleiman RJ, Kimmel LH, Bove SE, Lanz TA, Harms JF, Romegialli A, Miller KS, Willis A, des ES, Kuhn M, Schmidt CJ (2011) Chronic suppression of phosphodiesterase 10A alters striatal expression

of genes responsible for neurotransmitter synthesis, neurotransmission, and signaling pathways implicated in Huntington's disease. J Pharmacol Exp Ther 336:64-76.

Klevytska AM, Tebbenkamp AT, Savonenko AV, Borchelt DR (2010) Partial depletion of CREB-binding protein reduces life expectancy in a mouse model of Huntington disease. J Neuropathol Exp Neurol 69:396-404.

Lastres-Becker I, Bizat N, Boyer F, Hantraye P, Fernandez-Ruiz J, Brouillet E (2004) Potential involvement of cannabinoid receptors in 3-nitropropionic acid toxicity in vivo. Neuroreport 15:2375-2379.

Lastres-Becker I, Hansen HH, Berrendero F, de Miguel R., Perez-Rosado A, Manzanares J, Ramos JA, Fernandez-Ruiz J (2002) Alleviation of motor hyperactivity and neurochemical deficits by endocannabinoid uptake inhibition in a rat model of Huntington's disease. Synapse 44:23-35.

Leuti A, Laurenti D, Giampa C, Montagna E, Dato C, Anzilotti S, Melone MA, Bernardi G, Fusco FR (2013) Phosphodiesterase 10A (PDE10A) localization in the R6/2 mouse model of Huntington's disease. Neurobiol Dis 52:104-116.

Likar B, Viergever MA, Pernus F (2001) Retrospective correction of MR intensity inhomogeneity by information minimization. IEEE Trans Med Imaging 20:1398-1410.

Loeckx D, Maes F, Vandermeulen D, Suetens P (2003) Nonrigid image registration using a statistical spline deformation model. In: Information Processing In Medical Imaging pp 463-474. St Martins College, Ambleside, UK.

Luesse HG, Schiefer J, Spruenken A, Puls C, Block F, Kosinski CM (2001) Evaluation of R6/2 HD transgenic mice for therapeutic studies in Huntington's disease: behavioral testing and impact of diabetes mellitus. Behav Brain Res 126:185-195.

Luthi-Carter R, Strand A, Peters NL, Solano SM, Hollingsworth ZR, Menon AS, Frey AS, Spektor BS, Penney EB, Schilling G, Ross CA, Borchelt DR, Tapscott SJ, Young AB, Cha JH, Olson JM (2000) Decreased expression of striatal signaling genes in a mouse model of Huntington's disease. Hum Mol Genet 9:1259-1271.

Luyten L, Casteels C, Vansteenwegen D, Van Kuyck K, Koole M, Van Laere K, Nuttin B (2012) Micro-positron emission tomography imaging of rat brain metabolism during expression of contextual conditioning. J Neurosci 32:254-263.

Maes F, Collignon A, Vandermeulen D, Marchal G, Suetens P (1997) Multimodality image registration by maximization of mutual information. IEEE Trans Med Imaging 16:187-198.

Mangiarini L, Sathasivam K, Seller M, Cozens B, Harper A, Hetherington C, Lawton M, Trottier Y, Lehrach H, Davies SW, Bates GP (1996) Exon 1 of the HD gene with an expanded CAG repeat is sufficient to cause a progressive neurological phenotype in transgenic mice. Cell 87:493-506.

McCaw EA, Hu H, Gomez GT, Hebb AL, Kelly ME, ovan-Wright EM (2004) Structure, expression and regulation of the cannabinoid receptor gene (CB1) in Huntington's disease transgenic mice. Eur J Biochem 271:4909-4920.

Metz GA, Whishaw IQ (2002b) Drug-induced rotation intensity in unilateral dopamine-depleted rats is not correlated with end point or qualitative measures of forelimb or hindlimb motor performance. Neuroscience 111:325-336.

Metz GA, Whishaw IQ (2002a) Cortical and subcortical lesions impair skilled walking in the ladder rung walking test: a new task to evaluate fore- and hindlimb stepping, placing, and co-ordination. J Neurosci Methods 115:169-179.

Nicolas G, Devys D, Goldenberg A, Maltete D, Herve C, Hannequin D, Guyant-Marechal L (2011) Juvenile Huntington disease in an 18-month-old boy revealed by global developmental delay and reduced cerebellar volume. Am J Med Genet A 155A:815-818.

Nishi A, Kuroiwa M, Miller DB, O'Callaghan JP, Bateup HS, Shuto T, Sotogaku N, Fukuda T, Heintz N, Greengard P, Snyder GL (2008) Distinct roles of PDE4 and PDE10A in the regulation of cAMP/PKA signaling in the striatum. J Neurosci 28:10460-10471.

Petr GT, Schultheis LA, Hussey KC, Sun Y, Dubinsky JM, Aoki C, Rosenberg PA (2013) Decreased expression of GLT-1 in the R6/2 model of Huntington's disease does not worsen disease progression. Eur J Neurosci 38:2477-2490.

Poisnel G, Herard AS, El Tannir El TN, Bourrin E, Volk A, Kober F, Delatour B, Delzescaux T, Debeir T, Rooney T, Benavides J, Hantraye P, Dhenain M (2012) Increased regional cerebral glucose uptake in an APP/PS1 model of Alzheimer's disease. Neurobiol Aging 33:1995-2005.

Qi J, Leahy RM, Cherry SR, Chatziioannou A, Farquhar TH (1998) High-resolution 3D Bayesian image reconstruction using the microPET small-animal scanner. Phys Med Biol 43:1001-1013.

Rattray I, Smith E, Gale R, Matsumoto K, Bates GP, Modo M (2013) Correlations of behavioral deficits with brain pathology assessed through longitudinal MRI and histopathology in the R6/2 mouse model of HD. PLoS One 8:e60012.

Reiner A, Albin RL, Anderson KD, D'Amato CJ, Penney JB, Young AB (1988) Differential loss of striatal projection neurons in Huntington disease. Proc Natl Acad Sci U S A 85:5733-5737.

Richfield EK, Herkenham M (1994) Selective vulnerability in Huntington's disease: preferential loss of cannabinoid receptors in lateral globus pallidus. Ann Neurol 36:577-584.

Richfield EK, Maguire-Zeiss KA, Vonkeman HE, Voorn P (1995) Preferential loss of preproenkephalin versus preprotachykinin neurons from the striatum of Huntington's disease patients. Ann Neurol 38:852-861.

Ross CA, Tabrizi SJ (2011) Huntington's disease: from molecular pathogenesis to clinical treatment. Lancet Neurol 10:83-98.

Ruocco HH, Lopes-Cendes I, Laurito TL, Li LM, Cendes F (2006) Clinical presentation of juvenile Huntington disease. Arq Neuropsiquiatr 64:5-9.

Samadi P, Boutet A, Rymar VV, Rawal K, Maheux J, Kvann JC, Tomaszewski M, Beaubien F, Cloutier JF, Levesque D, Sadikot AF (2013) Relationship between BDNF expression in major striatal afferents, striatum morphology and motor behavior in the R6/2 mouse model of Huntington's disease. Genes Brain Behav 12:108-124.

Sawiak SJ, Wood NI, Williams GB, Morton AJ, Carpenter TA (2009) Voxel-based morphometry in the R6/2 transgenic mouse reveals differences between genotypes not seen with manual 2D morphometry. Neurobiol Dis 33:20-27.

Seeger TF, Bartlett B, Coskran TM, Culp JS, James LC, Krull DL, Lanfear J, Ryan AM, Schmidt CJ, Strick CA, Varghese AH, Williams RD, Wylie PG, Menniti FS (2003) Immunohistochemical localization of PDE10A in the rat brain. Brain Res 985:113-126.

Suarez J, Bermudez-Silva FJ, Mackie K, Ledent C, Zimmer A, Cravatt BF, de Fonseca FR (2008) Immunohistochemical description of the endogenous cannabinoid system in the rat cerebellum and functionally related nuclei. J Comp Neurol 509:400-421.

The Huntington's Disease Collaborative Research Group (1993) A novel gene containing a trinucleotide repeat that is expanded and unstable on Huntington's disease chromosomes. The Huntington's Disease Collaborative Research Group. Cell 72:971-983.

Van Laere K, Casteels C, Dhollander I, Goffin K, Grachev I, Bormans G, Vandenberghe W (2010) Widespread decrease of type 1 cannabinoid receptor availability in Huntington disease in vivo. J Nucl Med 51:1413-1417.

Van Laere KJ, Versijpt J, Koole M, Vandenberghe S, Lahorte P, Lemahieu I, Dierckx RA (2002) Experimental performance assessment of SPM for SPECT neuroactivation studies using a subresolution sandwich phantom design. Neuroimage 16:200-216.

Vandeputte C, Taymans JM, Casteels C, Coun F, Ni Y, Van Laere K, Baekelandt V (2010) Automated quantitative gait analysis in animal models of movement disorders. BMC Neurosci 9:11-92.

Vonsattel JP, Myers RH, Stevens TJ, Ferrante RJ, Bird ED, Richardson EP, Jr. (1985) Neuropathological classification of Huntington's disease. J Neuropathol Exp Neurol 44:559-577.

Wooley CM, Xing S, Burgess RW, Cox GA, Seburn KL (2009) Age, experience and genetic background influence treadmill walking in mice. Physiol Behav 96:350-361.

8. FIGURES LEGEND

Figure 1: Experiment time-line. Experiment time-line for functional and structural imaging of a transgenic mouse model in the pre-, early and late symptomatic phase of Huntington Disease (A). A detailed description of the different small-animal PET acquisitions conducted per week is shown in B. w, week; d, day

Figure 2: Mean [^{18}F]MK-9470, [^{18}F]JNJ42259152 and [^{18}F]FDG in R6/2. Average cross-sectional small-animal PET images of [^{18}F]MK-9470 (A), [^{18}F]JNJ42259152 (B) and [^{18}F]FDG (C) uptake in 11-12-week-old transgenic R6/2 mice and their wild-type littermates (WT). Small-animal PET images are overlayed on a MRI mouse brain template in Paxinos stereotactic space. Color bars indicate SUV for [^{18}F]MK-9470, BP_{ND} for [^{18}F]JNJ42259152 and relative intensity for [^{18}F]FDG. Note the lower uptake of [^{18}F]JNJ42259152 in the caudate-putamen bilaterally of 12-week-old R6/2 mice.

Figure 3: Relative [^{18}F]MK-9470 binding in R6/2. (A) Coronal (top 2 rows) and axial (bottom 3 rows) brain sections showing significantly decreased relative [^{18}F]MK-9470 binding in a cluster comprising the bilateral hippocampus, caudate-putamen, globus pallidus, thalamic nucleus, superior colliculus and cerebellum in R6/2 mice between 7 weeks and 5 weeks of age (n=8;figure given at p_{height}<0.005 uncorrected) as compared to WTs (n=7). (B) Coronal (top 2 rows) and axial (bottom 3 rows) brain sections showing significantly decreased relative [^{18}F]MK-9470 binding in the left hippocampus, globus pallidus, caudate-putamen, thalamic nucleus, superior colliculus and cerebellum in R6/2 mice between 11 weeks and 5 weeks of age (n=5;figure given at p_{height}<0.005 uncorrected) as compared to WTs (n=6). Significance is shown with a T statistic color scale, which corresponds to the level of significance at the voxel-level. The distance between coronal sections is 1.00 mm and between axial sections is 0.4 mm. Images are in neurological convention. No significant differences were observed using the pre-defined VOI analysis.

Figure 4: PDE10A in R6/2 (A) Coronal brain sections showing overlays on the regions with significantly decreased PDE10A binding potential in R6/2 mice between 5- and 11 weeks of age (n=5), as compared to WT animals (n=3) figure given at threshold p_{height} < 0.005). Significant clusters are shown using a T-statistic color scale, which corresponds to the level of significance at the voxel level. A transverse and sagittal section with the intersection point set to the Paxinos coordinate peak max,

i.e. the left caudate-putamen is shown on the right. Images are in neurological convention (L=left; R= right). (B) Histograms of BP_{ND} values of the bilateral caudate-putamen in R6/2 and WT animals over time. Data were obtained using a pre-defined VOI analysis. Data are shown as mean ± SD. 2-way ANOVA; *p<0.05; ***p<0.001

Figure 5: Balance and motor coordination on the rotarod R6/2 and WT mice were subjected to 5 different speeds on a fixed speed rotarod, receiving two trials per speed. The mean±SD of the duration of balance or the latency to fall (maximum trial length = 60 sec) for the two trials at the lowest (16 rpm) and highest speed (32 rpm) is shown.. R6/2 mice exhibited a decline in latency to fall from the rotarod with age, reaching statistical significance at 13 weeks of age. 2-way ANOVA; *p<0.05; **p<0.01; ***p<0.001

Figure 6: (A-B) Gait parameters of the Catwalk (A) Histograms of swing speed, stride length, print area and stand at week 13. Statistical analysis revealed for these parameters an effect of genotype at that age. Data are shown as mean ± SD. (B) Representative examples of the step-pattern of a R6/2 mouse *(top row)* and a WT animal *(bottom row)*. Note the shorter stride length for R6/2 as indicated by the full line. FP, forepaw; HP, hindpaw; L, left; R; right **(C) Quantitative outcome on the irregular horizontal ladder looking at the front paw** Graphs of the number of errors and the error sore between R6/2 mice *(dotted line)* and WT littermates *(full line)* at week 6, 9 and 13 are shown. Data are shown as mean ± SD.

Figure 7 (A-B) Relative [^{18}F]MK-9470 binding and motor function (A) Voxel-based correlation analyses results of the difference in relative [^{18}F]MK-9470 binding with rotarod performance (32 rpm) at 13 weeks of age. Significance is shown with a T statistic color scale, which corresponds to the level of significance at the voxel-level. Images are in neurological orientation. (B) Scatter plot of difference in relative [^{18}F]MK-9470 binding at the maximal peak location (i.e. (x, y, z)=(-1.4, -0.6,-1.2)) in the hippocampus in relation to the latency to fall on a 32 rpm speed rotarod at 13 weeks of age. **(C-D) PDE10A and motor function** Scatter plot of right caudate-putamen BP_{ND} values in relation to (A) the print area (mm^3) and (B) the duration of stand (s) of the left forepaw, as measured using the Catwalk. **(E-F) PET quantification by predefined VOI map vs. MR-based segmentation** Relationship of absolute [^{18}F]MK-9470 values (A; r=0.94, p<0.0001) and of BP_{ND} values (B; r=0.97, p<0.0001) in the

caudate-putamen determined by a predefined VOI map oriented in Paxinos space and individual MR-based segmentation in native space.

9. TABLES

Table 1: Peak locations for the clusters in the group comparisons and correlation analysis

(at $p_{height} \leq 0.005$ uncorrected, $k_E > 200$)

	Cluster-level		Voxel-level			Structure			Name
	p_{corr}	k_E	T	p_{uncorr}	Intensity Difference (%)	x	y	z	
[^{18}F]MK-9470 – CB1 Receptor									
R6/2 < WT: week 5	<0.001	4199	6.17	<0.001	-8.1± 2.6 %	-2.8	-1.0	-4.0	Bilateral globus pallidus, caudate-putamen and thalamic nucleus
			5.11	<0.001		-1.4	-1.2	-5.4	
			5.05	<0.001		-0.2	-3.2	-5.0	
R6/2 Δ(7 weeks – 5 weeks) < WT Δ(7 weeks – 5 weeks)	<0.001	6326	9.69	<0.001	-11.6 ± 2.0 %	-2.0	-2.4	-2.8	Bilateral hippocampus, globus pallidus, caudate-putamen, superior colliculus, thalamic nucleus and cerebellum
			8.91	<0.001		1.0	-3.8	-1.6	
			8.51	<0.001		0.8	-2.0	-3.2	
R6/2 Δ(11 weeks – 5 weeks) < WT Δ(11 weeks – 5 weeks)	0.001	2198	7.50	<0.001	-13.7 ± 3.1 %	1.6	-4.4	-1.8	Left hippocampus, globus pallidus, caudate-putamen, superior colliculus, thalamic nucleus and cerebellum
			5.41	<0.001		2.4	-2.8	-3.0	
			4.72	<0.001		-0.4	-5.8	-2.0	

[^{18}F]JNJ42259152 – PDE10A									
R6/2 Δ(11 weeks – 5 weeks) < WT Δ(11 weeks – 5 weeks)	0.001	383	11.74	<0.001	-67.9 ± 1.0 %	-2.8	0.2	-3.6	Right caudate-putamen
			5.66	0.002		-1.2	1.2	-4.0	
	<0.001	561	9.93	<0.001	-79.1 ± 1.9%	1.4	0.0	-3.0	
			9.76	<0.001		1.8	0.2	-3.8	Left caudate-putamen
			6.40	0.002		1.0	1.2	-4.4	
Correlation Analysis									
[^{18}F]MK-9470: positive correlation with latency to fall on Rotarod (32 rpm) at 13 weeks	0.006	790	8.81	<0.001	-	-1.4	-0.6	-1.2	Bilateral hippocampus and primary sensory cortex
			5.58	<0.001		1.6	-0.8	-1.6	
			5.07	<0.001		-1.6	0.8	-1.6	

P_{corr} at cluster level: the chance (p) of finding a cluster with this or a greater size (k_E), corrected for search volume

k_E = cluster extent

T = measure of the statistical significance

P_{uncorr} at voxel level: the chance (p) of finding (under the null hypothesis) a voxel with this or a greater height (T-statistic), uncorrected for search volume

% = intensity difference at the voxel level of R6/2 rats in comparison to controls

x = lateral distance in mm from the midline (negative values to the right side)

y = anteroposterior location relative to Bregma (negative values: posterior to Bregma)

z = dorsoventral position (based upon the Paxinos stereotactic atlas).

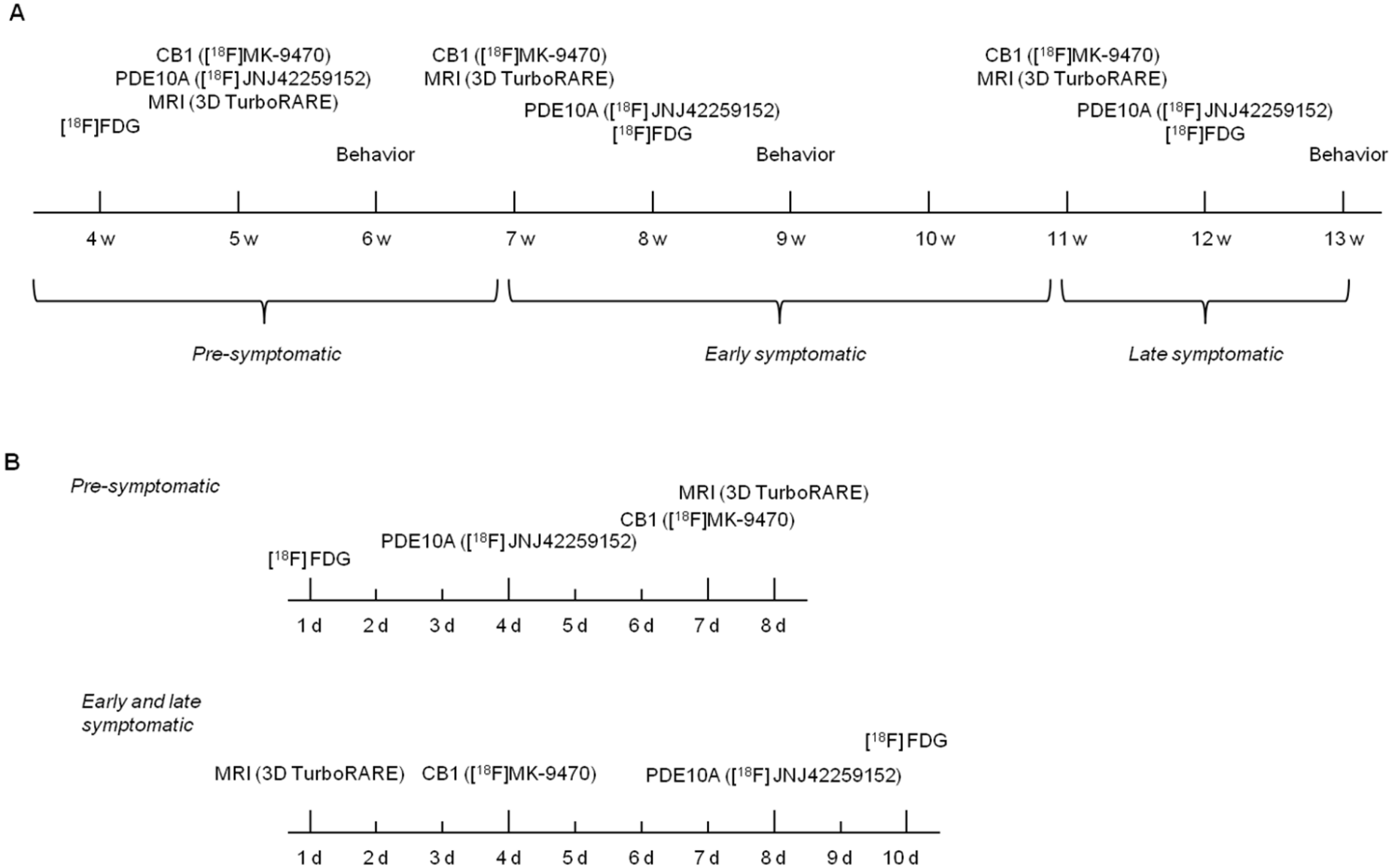
A
CB1 ([18F]MK-9470)
PDE10A ([18F] JNJ42259152)
MRI (3D TurboRARE)
[18F]FDG
Behavior
CB1 ([18F]MK-9470)
MRI (3D TurboRARE)
PDE10A ([18F] JNJ42259152)
[18F]FDG
Behavior
CB1 ([18F]MK-9470)
MRI (3D TurboRARE)
PDE10A ([18F] JNJ42259152)
[18F]FDG
Behavior
4 w
5 w
6 w
7 w
8 w
9 w
10 w
11 w
12 w
13 w
Pre-symptomatic
Early symptomatic
Late symptomatic
B
Pre-symptomatic
MRI (3D TurboRARE)
CB1 ([18F]MK-9470)
PDE10A ([18F] JNJ42259152)
[18F] FDG
1 d
2 d
3 d
4 d
5 d
6 d
7 d
8 d
Early and late symptomatic
[18F] FDG
MRI (3D TurboRARE)
CB1 ([18F]MK-9470)
PDE10A ([18F] JNJ42259152)
1 d
2 d
3 d
4 d
5 d
6 d
7 d
8 d
9 d
10 d

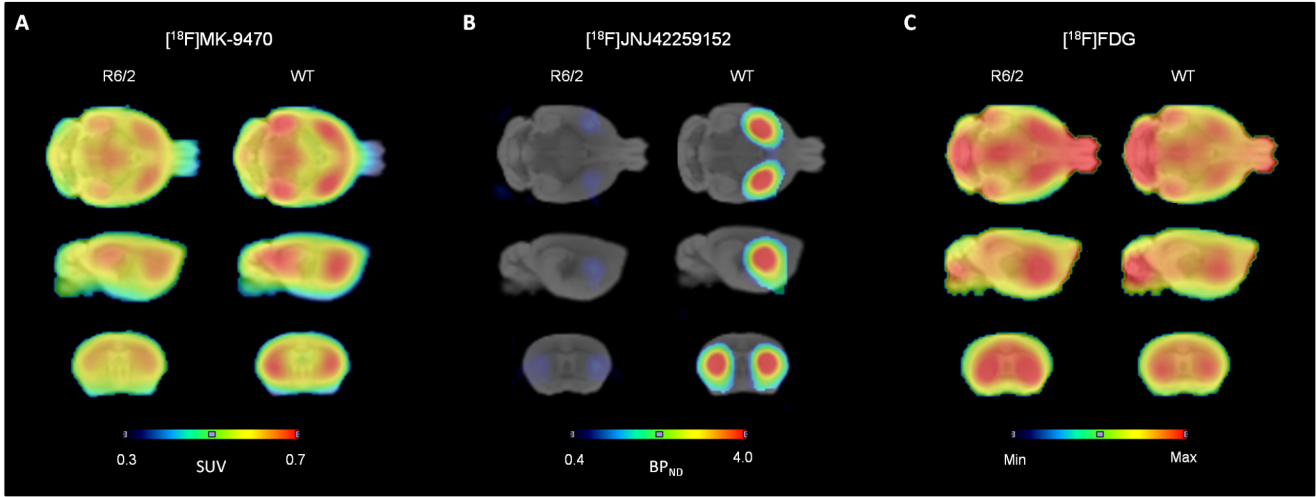
A
[18F]MK-9470
R6/2
WT
0.3
SUV
0.7
B
[18F]JNJ42259152
R6/2
WT
0.4
BPND
4.0
C
[18F]FDG
R6/2
WT
Min
Max

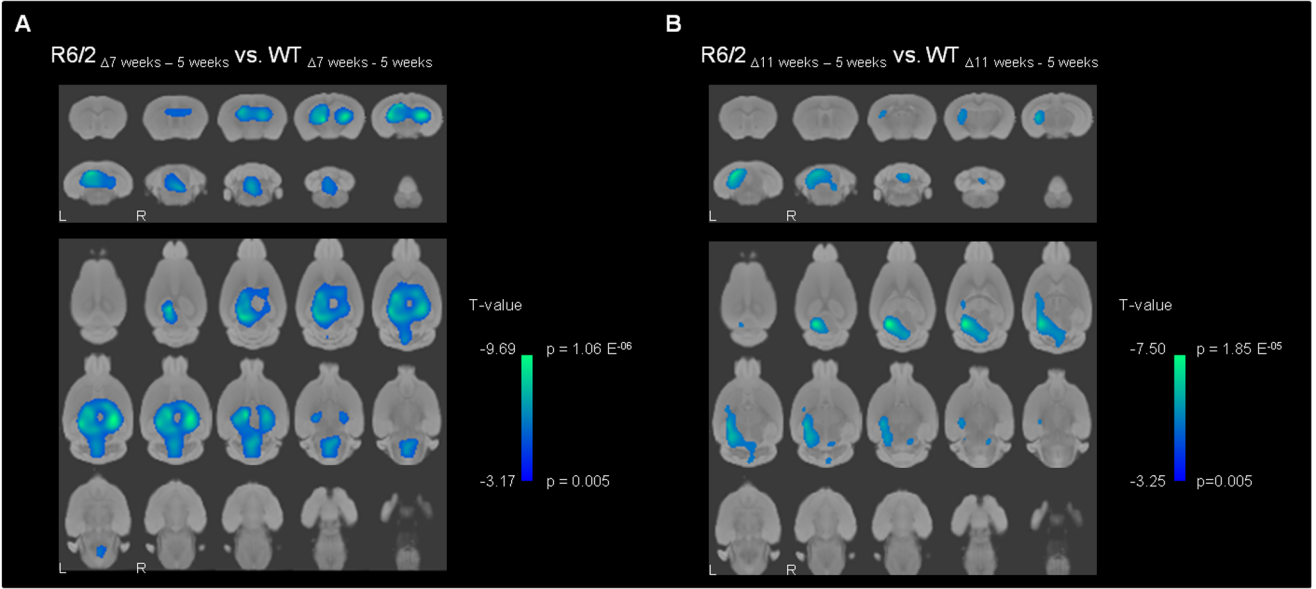
A
R6/2 Δ7 weeks – 5 weeks vs. WT Δ7 weeks - 5 weeks
L
R
T-value
-9.69
p = 1.06 E-06
-3.17
p = 0.005
B
R6/2 Δ11 weeks – 5 weeks vs. WT Δ11 weeks - 5 weeks
T-value
-7.50
p = 1.85 E-05
-3.25
p=0.005

A

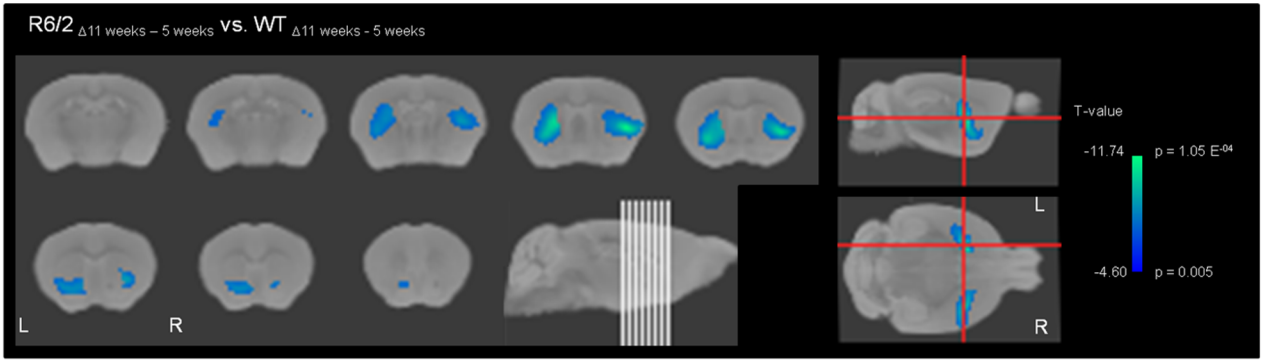
R6/2 Δ11 weeks – 5 weeks vs. WT Δ11 weeks - 5 weeks
T-value
-11.74
p = 1.05 E-04
-4.60
p = 0.005
L
R
L
R

B

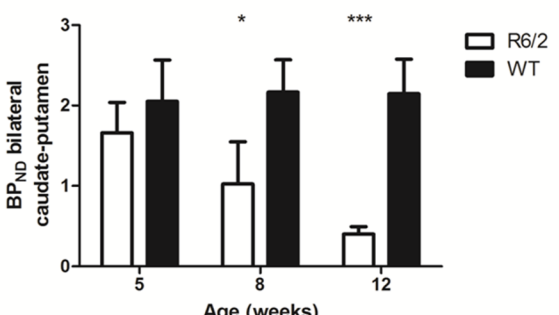
BPND bilateral caudate-putamen
3
2
1
0
*
***
R6/2
WT
5
8
12
Age (weeks)

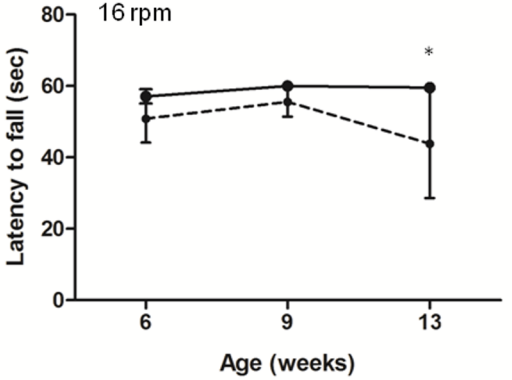
16 rpm
80
60
40
20
0
Latency to fall (sec)
*
6
9
13
Age (weeks)

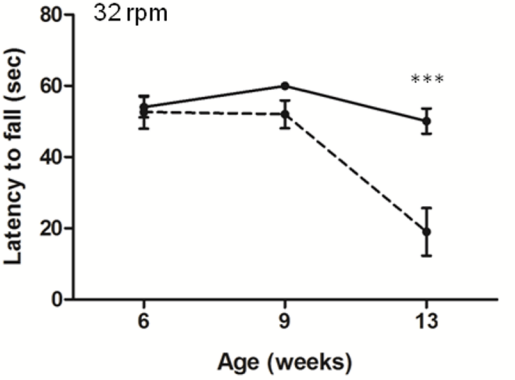
32 rpm
80
60
40
20
0
Latency to fall (sec)
***
6
9
13
Age (weeks)

WT
R6/2

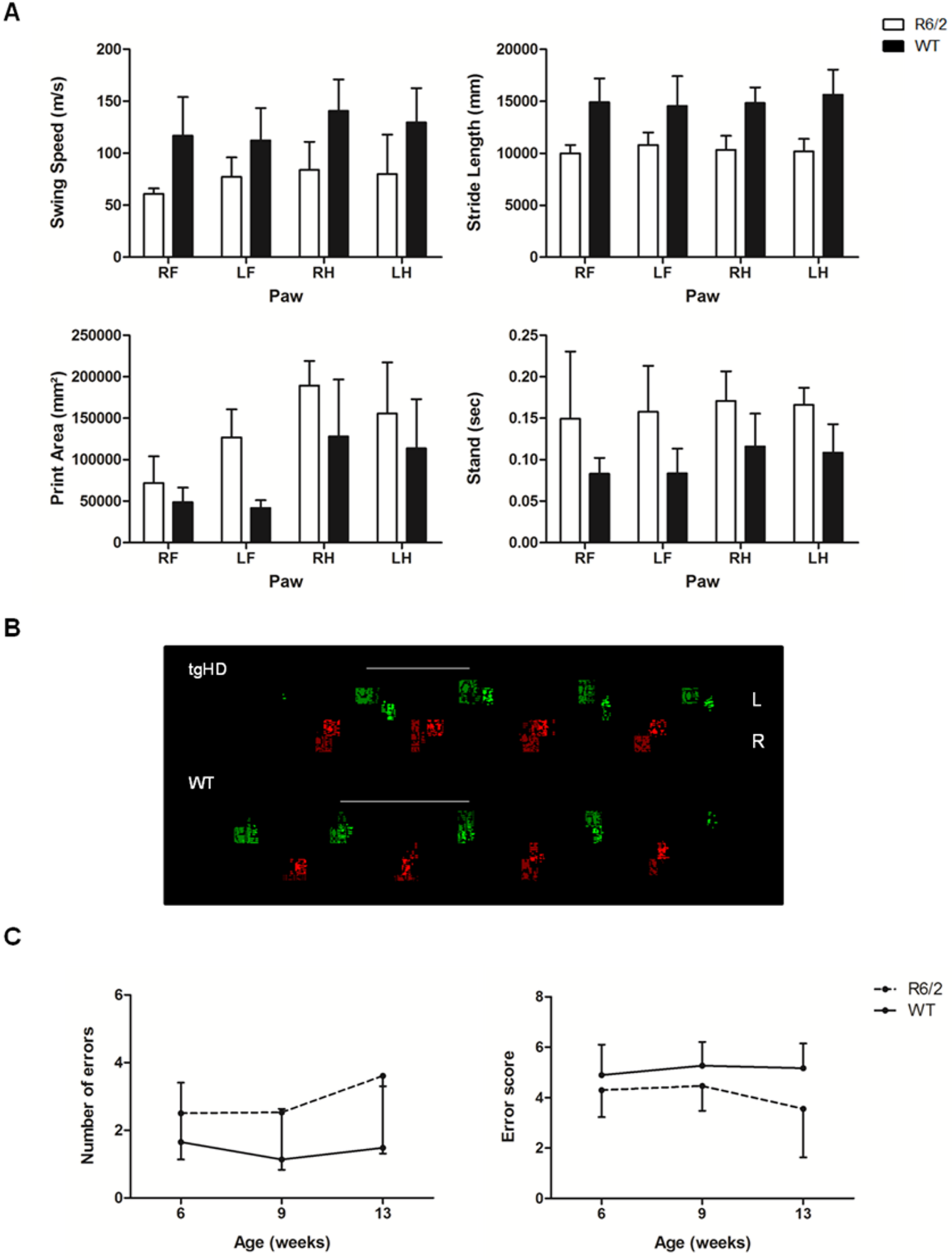
A
R6/2
WT
Swing Speed (m/s)
200
150
100
50
0
RF
LF
RH
LH
Paw
Stride Length (mm)
20000
15000
10000
5000
0
RF
LF
RH
LH
Paw
Print Area (mm²)
250000
200000
150000
100000
50000
0
RF
LF
RH
LH
Paw
Stand (sec)
0.25
0.20
0.15
0.10
0.05
0.00
RF
LF
RH
LH
Paw
B
tgHD
WT
L
R
C
R6/2
WT
Number of errors
6
4
2
0
6
9
13
Age (weeks)
Error score
8
6
4
2
0
6
9
13
Age (weeks)

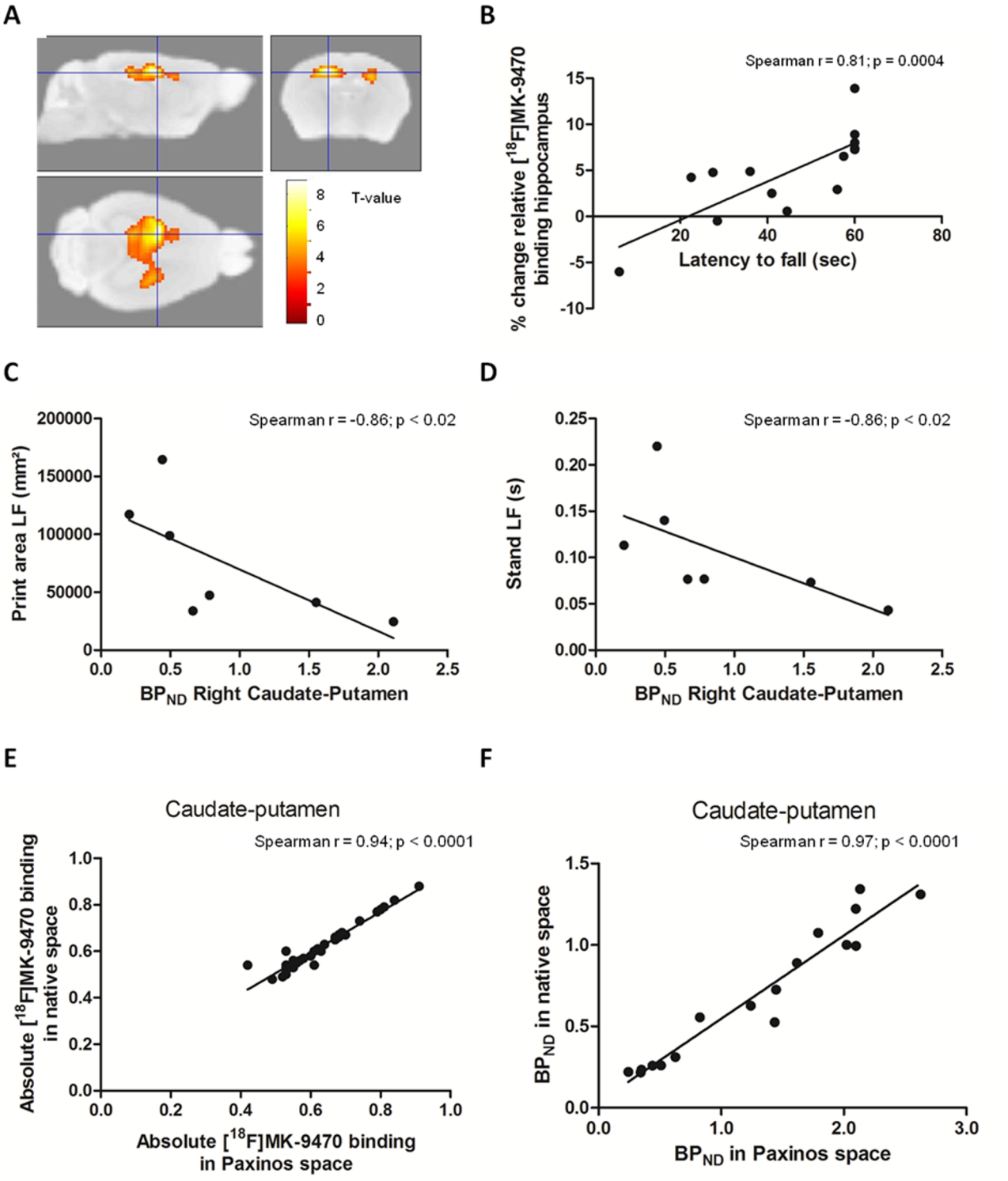
A
T-value
8
6
4
2
0
B
Spearman r = 0.81; p = 0.0004
% change relative [18F]MK-9470 binding hippocampus
Latency to fall (sec)
C
Spearman r = -0.86; p < 0.02
Print area LF (mm²)
BPND Right Caudate-Putamen
D
Spearman r = -0.86; p < 0.02
Stand LF (s)
BPND Right Caudate-Putamen
E
Caudate-putamen
Spearman r = 0.94; p < 0.0001
Absolute [18F]MK-9470 binding in native space
Absolute [18F]MK-9470 binding in Paxinos space
F
Caudate-putamen
Spearman r = 0.97; p < 0.0001
BPND in native space
BPND in Paxinos space